The reconstruction and functional mapping of a recurrent microcircuit in *Drosophila* mushroom body

Guangxia Wang[1,2,*#], Bangyu Zhou[,1,2], Shengxiong Wang[2,3], Kai Yang[1,2], Jianjian Zhao[1,2], Xing Yang[1,2], Yiming Li[1,2], Lijun Shen[4]

[1]Institute of Neuroscience and State Key Laboratory of Neuroscience, Center for Excellence in Brain Science and Intelligence Technology, Chinese Academy of Science, Shanghai 20003, China

[2]University of Chinese Academy of Sciences, Shanghai 200031, China

[3]State key Laboratory of Brain and Cognitive Science, Institute of Biophysics, Chinese Academy of Science, Beijing 10010, China

[4]Institute of Automation, Chinese Academy of Sciences, Beijing 10090, China

[#]First Author

***For Corresponding: Guangxia Wang**, **wangguangxia121@126.com,**

http://orcid.org/0000-0003-0964-6601

Abstract

In *Drosophila melanogaster*, mushroom body and anterior paired lateral (APL) neurons play important roles not only in learning and memory but also in high cognitive behavior, reversal learning. The circuit between APL neurons and Kenyon cells (KCs) in the mushroom body underlies this behavior, including reversal learning, and electron microscopy (EM) methods must be used to reveal this circuit. Here, we reconstructed the connections between mushroom body cells and APL neurons in the vertical lobe of the mushroom body via focused ion beam scanning electron microscopy (FIB-SEM) and sparse genetic horseradish peroxidase (HRP) labeling. We offer the first EM evidence that recurrent network and lateral inhibition connections exist between APL neurons and KCs in the vertical lobe of the mushroom body. This circuit is the neural basis of action selection decision making, associative learning and reversal learning. Additionally, dopamine neurons project to different areas of mushroom bodies and, together with extrinsic neurons and KC axons, form a compartmental structure of mushroom body axons, thereby restricting the KC-mushroom body output neuron (MBON) response to local compartments. Whether APL neurons also respond locally is uncertain. We found that APL neurons exhibited input and output synapses that were intermixed and arranged on enlarged and thin sections, respectively, resembling a string of beads. Different KCs were found to project to APL neurons nonrepetitively, forming a local circuit structure. Furthermore, using a single neurite calcium imaging method, we identified local calcium domains on this circuit, suggestive of individual electrical compartments. The electrically recorded APL neurons were nonspike neurons that selectively responded to odor in both the lobes and calyx. Thus, the localized APL neuron responses coordinate with mushroom body–dopamine-MBON compartmental function.

Introduction

Mushroom bodies are the most important structures in *Drosophila* and are primarily composed of KCs (KCs). The cell bodies and dendrites of three different intrinsic neurons constitute the calyx, and the axons constitute the peduncle and three lobes, the αβ, α′β′, and γ lobes (Tanaka, Tanimoto, & Ito, 2008). Mushroom bodies are the third level of the olfactory system; they receive input from projection neurons in the calyx and send information through contacts with extrinsic neurons in the lobes (Aso et al., 2014a, 2014b).

A pair of symmetrically distributed GABAergic interneurons, called anterior posterior lateral (APL) neurons, each of which sends out two branches, innervate both the calyx and lobes of mushroom bodies. APL neurons are thought to function similarly to their homolog giant GABAergic neurons (GGNs) in the locust, which receive information in the calyx of the mushroom body and send global feedback inhibition to KCs in the lobes (Papadopoulou, Cassenaer, Nowotny, & Laurent, 2011). APL neurons and mushroom bodies participate in sparse odor coding (Lei, Chen, Li, Liu, & Guo, 2013), olfactory learning inhibition (Liu & Davis, 2009), mutual odor inhibition, visual reversal learning (Ren, Li, Wu, Ren, & Guo, 2012), olfactory reversal learning (Wu, Ren, Li, & Guo, 2012), decorrelated odor coding (Lin, Bygrave, de Calignon, Lee, & Miesenbock, 2014), and visual decision making. Both blocking APL neuron transmission and decreasing the expression of GABAA receptors in the αβ lobe of mushroom bodies inhibit visual reversal learning in *Drosophila* (Ren et al., 2012). Recent studies have demonstrated that APL neurons coexpress octopamine and GABA (Pitman et al., 2011). Further studies found that octopaminergic APL neurons project to the α′β′ lobe of mushroom bodies in the mushroom body output neuron (MBON)-β′2mp pathway and serotonergic dorsal paired medial (DPM) neurons

project to the αβ lobe of mushroom bodies in the MBON-β2β′2a pathway to mediate 3-h anesthesia-sensitive memory (Pitman et al., 2011; Yang et al., 2016).

Some neuromodulator neurons innervate mushroom bodies, and dopaminergic neurons might mediate unconditional stimuli, such as reward and punishment during learning. Dopamine neurons couple with KCs, which encode odor information for conditioning, learning and storage of olfactory information.

Dopaminergic and extrinsic neurons have been shown to project to different areas of mushroom body lobes and separate mushroom bodies into 15 functional compartments (Aso et al., 2014a, 2014b). The dopamine neurons that project locally encode innate states as well as external experiences. Together with KC axons and extrinsic neurons, the locally projecting dopamine neurons form local information circuits in this area (Cohn, Morantte, & Ruta, 2015), dopamine neurons constrain KC neuron responding locally.

Studies on APL neuron morphology have shown that these neurons innervate whole lobes and the calyx (Liu & Davis, 2009), and both presynapses and postsynapses of APL neurons are found in all these areas. APL neurons with KC neurons play roles in numerous high cognitive behaviors, and the following questions remain unanswered: What are the neural circuits of APL neurons and KCs that underlie these behaviors? Does a local circuit also exist between APL and KCs? Since DA-KC-MBON circuit function locally, APL neurons intermixed with mushroom body are also well segmented via DA neurons. Moreover, APL neurons are activated via KC neurons which have locally response at the vertical lobe. Do APL neurons function locally at lobe and calyx?

To explore these questions, we introduced a 3D electron microscopy (EM) reconstruction method to obtain information at the nanoscale. We genetically labeled APL neurons with horse-

radish peroxidase (HRP) and examined the circuit using focused ion beam series electron microscopy (FIB-SEM). We obtained substantial amounts of continuous EM data in the mushroom body vertical lobe (volume EM data) and then reconstructed APL neurons and their connectomes. We found that APL neurites received KC input and then KC sent out information to APL neurites, forming a recurrent loop. We showed that individual APL neurites have intermixed presynapses and postsynapses that are found on alternate arranged enlarged and thin segments, respectively. Thus structure constitutes the electrically separation on APL single neurite, forming a local information flow from KC to enlargement of APL and send out information from thin part of APL to other KC. The structural evidence supports the potential existence of a local circuit between APL neurons and KCs. Electrophysiological recording revealed that APL neurons elicit nonspikes. In addition, via a calcium imaging method used to indicate neuron activity, we observed calcium domains on individual APL neurites, suggesting that signal propagation is limited on these neurites and that this electrical segmentation is underscored by the enlargement and thinning of the neurite. APL neurons send out odor-dependent signals locally in both the calyx and the lobes. These data support the hypothesis that a local circuit but not a global circuit exists between APL neurons and KCs in mushroom bodies, which complements the compartmental structure of mushroom bodies and might enable the various inhibitory local circuits associated with learning and innate behavior and other behavior. Thus, we supply the first EM evidence that local APL-KC neurons forms a recurrent network that is the neural basis of learning, reversal learning, and decision-making behavior.

Results

111 ***Three-dimensional reconstruction of HRP-labeled APL neurons and their connections in the***
112 ***mushroom body vertical lobe***

113 To explore the specific APL neurons and their connectomes, volume EM reconstruction was
114 applied. Because several high cognitive behaviors are based in the vertical lobe, we explored the
115 connectomes in this region. Two strategies are available for studying a target neuron and its con-
116 nections: one strategy is constructing all of the neurons in a specific brain area and then identify-
117 ing the target neuron and its connections (Macpherson et al., 2015), thus dense reconstruction.
118 The other strategy is sparse reconstruction (Kasthuri et al., 2015), in which neurons of interest
119 are sparse labeled and their connections are identified directly. The second strategy is much less
120 time consuming, providing us with the opportunity to identify our circuit of interest. In our study,
121 the classic EM tracer HRP was applied as a labeling method. We drive HRP (*UAS-HRP-mCD8-*
122 *GFP*) expression via *GH146-Gal4* to specifically labeling APL neurons at the mushroom body.
123 HRP catalyzes the formation of a 3,3'-diaminobenzidine (DAB) polymer (Joesch et al., 2016;
124 Kasthuri et al., 2015), which binds osmium to increase the electron density. FIB-SEM then ena-
125 bled us to obtain volume EM data of the vertical lobe of mushroom body from tip to bottom, ap-
126 proximately 30 (X) × 37 (Y) × 52 (Z) μm^3 (Fig. S1) and 40 nm thick per image.

127 The APL neurons expressing HRP exhibited deeper and darker membranes than other neu-
128 rons after EM preparation (Fig. 1A1 and A2), and our serial EM data allowed for synapse identi-
129 fication across several layers (Fig. 1B1-B6). With a work group comprising 5 people, we applied
130 strict standards to identify synapses and neurons across layers. Drosophila synapses contains
131 three components: a T-bar and vesicle at the presynpase and a darkened membrane at the
132 postsynapse (Marta et al., 2011), which have been identified across several layers of EM data.
133 Some labeled APL neurons showed darkened membranes that continued across several layers of

the EM data, whereas others showed darkened membranes that reappeared intermittently across layers. We marked the above as the APL neurons in our reconstruction work as criteria. To ensure that all data identified were accurate, we built a semiautomated workflow (Fig. S2, *Supplemental Material*). Only 100% positive data (all 5 people confirmed the data) were saved. After reconstructing an APL neuron and its pre- and postsynapses, we continued reconstructing the presynapse and postsynapse neuron skeleton of the APL neuron with the same standards. In the end, we obtained 3D reconstruction data for an APL neuron and its connection neurons in the vertical lobe (Fig. S3, Fig. 1G). In total, all reconstructed neurons and connections totaled 72432 nodes (nodes are labeled as the skeleton of neurons on each layer of EM data), 3968 μm of neurites, 183 neurites and 601 synapses (Table 1).

Table 1 Reconstruction data of APL connections in the mushroom body vertical lobe

(*) nodes represent the annotation of the APL skeleton, which is the component of the skeleton on each layer.

(**) represent the reconstruction results; not all synapses have an output neurite.

MB lobe	Neuron	Length (μm)	Nodes*	Neurites	Input synapse**	Output synapse**
α	APL	680	12190	22	96	103
	Input	1750	34090	71	60	198
	Output	332	6918	38	44	41
	Bidirectional	129	2646	4	7	17
α'	APL	930	13984	30	14	27
	Input	72	1273	8	0	8
	Output	75	1331	10	10	0

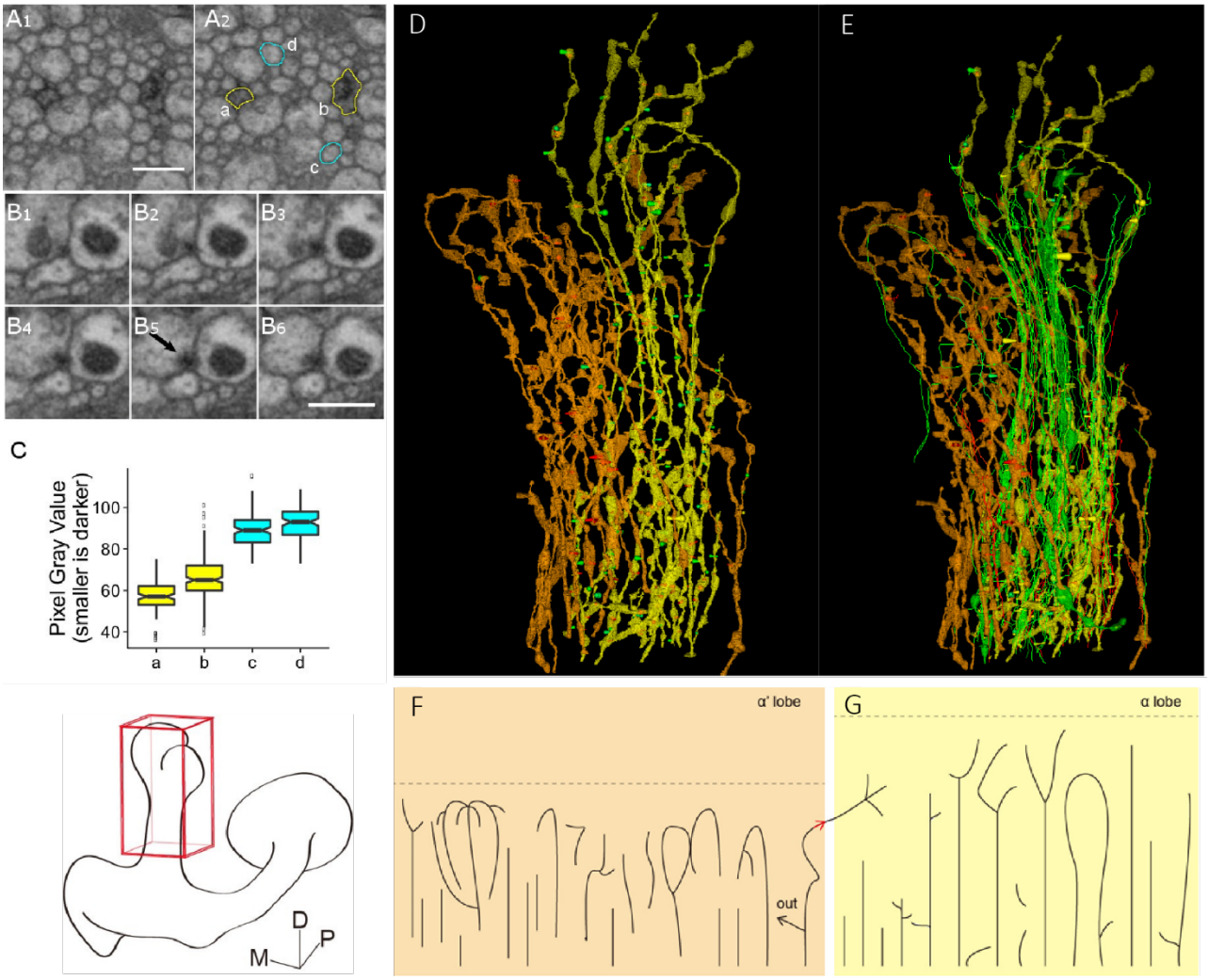

Fig. 1. Reconstruction of genetically labeled APL neurons and their connections in the mushroom body vertical lobe

(A) Two APL neurite branches with darkened membranes. In A2, yellow circles indicate membranes labeled with HRP in A1, while cyan circles indicate those not labeled. **(B)** Continuous synapse with T-bars. (B5) The arrow indicates a typical T-bar on this layer. The scale bar is 50 nm. **(C)** Pixel gray value measured in areas a, b, c, and d in A2. a and b are both darker than c and d. The scale bar is 500 nm. **(D)** 3D reconstructed APL neurite. **(E)** 3D reconstructed APL neurite and its connected neurite. **(D)** Top, dorsal. An APL neurite in the α lobe is shown in yel-

low, and an APL neurite in the α′ lobe is shown in orange. APL neurites in the α and α′ lobes have different trends, and they are sparse at the top of the mushroom body vertical lobe and dense in the middle. The green cone represents APL neurite input, and the red cone represents APL neurite output. **(E)** Those overlapping areas are not connected. In addition, the green neurite represents input neurons of APL neurites, and the red neurite represents output neurons of APL neurites. A few bidirectional neurons are also labeled green. Only skeletons of those neurons are displayed. **(F)** APL neurites in the α′ lobe. All constructed data contain 15 independent neurites longer than 12 μm. At the tip of the neurite, there are some horizontal connections and some complex branches, including a circle branch. There is one branch that receives input from neurons out of the mushroom body (labeled by the black arrow and the word out) and also projects to the α lobe. **(G)** APL neurites in the α′ lobe. There are 11 independent branches longer than 12 μm. Most APL neurites are vertical with simple branches, and the vertical branches have few horizontal connections unless near the top of the mushroom body vertical lobe. APL neurites less than 4 μm are omitted from this figure but had no branches.

APL neurites in the α and α′ lobes are independently, separated and exhibited obviously different trends (Fig. 1D). APL neurons penetrated into the inside of the vertical lobe of the mushroom body and dispersed more evenly in the horizontal direction. Overall, APL neurites in the vertical lobe do not appear as a complete net structure at we thought in previous study, at least in the α lobe. Firstly, we found only one connection between APL neurites in the α and α′ lobes, which also connected with APL branches going into the vertical lobe of mushroom body , and astrocytes are find to isolate α and α′ lobes under EM structure. Secondly, APL neurons in the top of the data set, i.e., the dorsal side of the vertical lobe of the mushroom body, were more sparse in the vertical direction. Fig. S4). A large proportion of these neurites extended in the ver-

185 tical direction (Fig. S5), consistent with the direction of the mushroom body neurons around
186 them. APL neurites in the α lobe extended straight upwards, while those in the α′ lobe spiraled
187 around those in the α lobe. Thirdly, there were more branches at the tip of the vertical lobe and
188 no branches at the stalk, especially in the α′ lobe. They are rarely separated and dependent neu-
189 rites at the stalk of the vertical lobe. These observations suggest that APL neurites in the α′ lobe
190 have much more complex connections than those in the α lobe. APL neurites in the α′ lobe ex-
191 tended more horizontally (Fig. S4), but the radius of APL neurites was approximately 10 nm
192 near the section interval, making tracing the APL horizontal branches in the α′ lobe difficult.
193 Therefore, we obtained less data on APL connections in the α′ lobe. In total, we observed 22
194 APL neurites in the α lobe, 30 APL neurites in the α′ lobe, 113 neurites connecting with APL
195 neurons in the α lobe, and 18 neurites connecting with APL neurons in the α′ lobe (Table 1). No-
196 tably, there were fewer than 20 APL branches in the horizontal section of the α lobe (Fig. S4,
197 Table 1) and approximately 1000 KCs in the α lobe; in contrast, there were fewer than 30 APL
198 branches in the α′ lobe (Fig. S4, Table 1) and approximately 300 KCs in the α′ lobe. These data
199 suggest that the average number of APL branches in the α lobe needs to be at least 50 to cover all
200 KCs, while the number of branches in the α′ lobe needs to be at least 10. The horizontal neurite
201 of APL, less than 40nm, might be missed in this dataset due to it below the lateral resolution of
202 EM. While indeed they are few in reality, because there are fewer neurites larger less than 40nm,
203 so neurites less than 40nm are rare. Evenly they exsits, the ability of chemical signal transduction
204 could be ignored due to the thinnest radius. Such, APL could not send signal globally but locally.
205 Due to the relative comprehensive reconstruction data of APL and its connections in the α
206 lobe, we further studied their neural connections next. We classified neurons connecting with
207 APL neurites into 3 groups based on the information flow between these neurons and APL neu-

208 rons. Neurons projecting to APL neurons were called input neurons, those that receive input
209 from APL neurites were called output neurons, and those that both project to APL neurites and
210 receive information from APL neurites were called bidirectional neurons. Among the input and
211 output neurons, over 60% formed a single contact with APL neurons. Those neurons extended
212 along APL neurons vertically in a bunch and then separated from APL neurons after forming a
213 synaptic contact at a distance. A few input neurons also formed two or three synaptic contacts
214 with APL neurons (Table 1).

215 In our reconstructed results, the total number of input synapses (presynapses) in the α lobe
216 was only approximately 100 (Table 1), which is far fewer than the total number of input synap-
217 ses needed to cover all KCs; even considering that our results underestimate the true situation by
218 four to five times (Fig. S6), we did not find enough input synapses to cover all KCs. Similar
219 conditions were observed in the output synapses (postsynapses) of APL neurons in the α lobe
220 and α' lobe. Thus, unlike the GGN in locusts, APL neurons in the vertical lobe do not seem to
221 act as broad inhibitory neurons, broadcasting inhibitory signals to all KCs, suggesting that the
222 physiological characteristics of GGNs may not be directly applicable to those of APL neurons.

223

224 ***APL pre- and postsynapses correlate with enlarged and thin neurite regions, respectively***

225 The neurites of APL neurons resembled a string of beads (Fig. 2A) with intermixed enlarged
226 and thin regions arranged on a single neurite, just as observed in the calyx (*unpublished data*).
227 Presynapses were mainly located in the enlarged regions, whereas postsynapses were mainly lo-
228 cated in the thin regions on APL single neurite (Fig. 2). Furthermore, mitochondria, which sup-
229 ply ATP for synapse release and vesicles, were located at the enlarged sections.

230

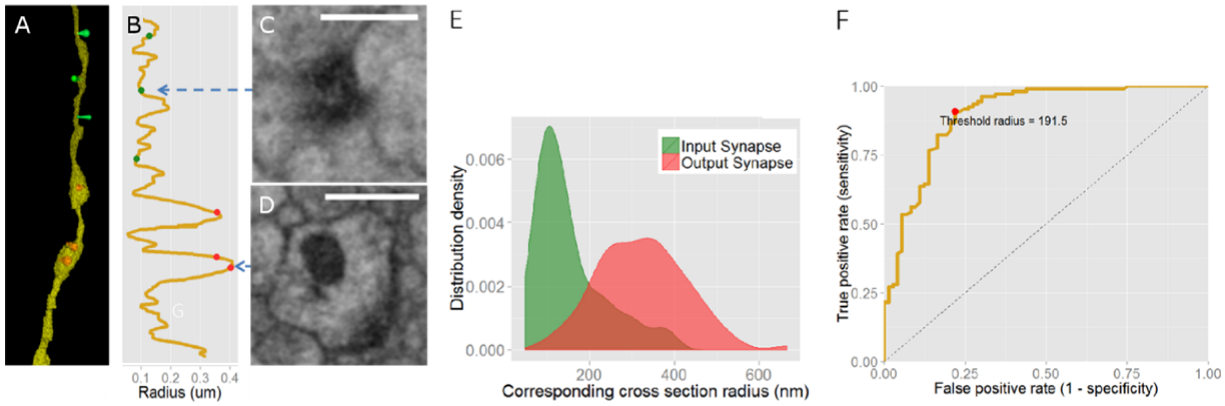

Fig. 2. Pre- and postsynapses located at both enlarged and thin regions of APL neurites. **(A)** 3D reconstructed segment of a single APL neurite, overall resembling a string of beads with intermixed enlarged and thin regions. The green cones indicate APL neurite input, while the red cones indicate APL neurite output. **(B)** Illustration of the section radius of the APL neurite in (A). The vertical axis represents the relative location of the APL neurite, and the horizontal axis represents the section radius of the APL neurite perpendicular to the relative location. In both A and B, the green cones represent input synapses, and the red cones represent output synapses. **(C)** A postsynapse at the thin part of the APL neurite. **(D)** A presynapse at the enlarged part of the APL neurite. In (C) and (D), the T-bar structure is distinguishable. The scale bar is 500 nm. **(E)** Distribution densities of section radii with input and output synapses across the APL neurite. The green curve represents the distribution density of section radii at input synapses. Most radii are approximately 100 nm, while a small number are larger. The red curve represents the distribution density of section radii at output synapses. The radii are widely distributed near 200 to 400 nm. **(F)** ROC curve to assess the direction of synapses using neurite section radii as the classifier. The curve shows a steep upward convex shape, indicating a high predictive accuracy of the direction using the synaptic radius. The red dot indicates the best classification threshold, 191.5 nm.

249 The diagonal line represents the performance of random classifiers to determine the direction of
250 each synapse.

251 We then examined whether the enlarged regions correlate with the location of APL neurite
252 presynapses. To answer this question, we first imaged the presynaptic proteins of APL neurons
253 under a light microscope with *GH146-Gal4* driving syb-GFP expression, revealing sparse puncta
254 of syb-GFP similar to those of the enlarged regions of APL neurons, and it hint a colocalization
255 between presynapse protein and enlargement part of APL neuorns (Fig. S9 and S10). We next
256 investigated the relationship between the radii of the APL neurites and synapse direction using
257 the EM dataset. We analyzed the distribution densities of input synapses (presynapses) and out-
258 put synapses (postsynapses) across APL neurite radii. In our dataset, the input and output syn-
259 apse peaks were clearly separated, with input synapses mainly centered at small radii (100 nm)
260 and output synapses mainly centered at large radii (300 nm) (Fig. 2E), indicating a correlation
261 between APL neurite radii and synapse direction. Therefore, we examined whether the radius of
262 an APL neurite could predict the direction of the synapse. To answer this question, we applied
263 receiver operating characteristics (ROC) analysis to assess synapse direction using the section
264 radius of the neurite as the classifier (Fig. 2F). The upward, steep shape of the ROC curve indi-
265 cated a high predictive accuracy, with the best separation point at 191.5 nm. This result shows
266 that the radii of APL neurites were highly correlated with synapse direction and that synapse di-
267 rection could be predicted based on neurite radius.

268 A previous study showed that pre- and postsynapses are located in both the lobes and the ca-
269 lyx, but whether they are located on the same neurite or on different neurites was unclear. Our
270 study confirmed that these synapses are located on the same neurite.

271 To display the mixed arrangement of the synapses in different directions of APL neurons and
272 compare among neurons, we excluded the distance between synapses and the length and branch-
273 es of neurons and extracted the topological arrangement between them. Here, we developed an
274 "*arrangement index*" (AI) to achieve this goal (*Supplemental Material*). Compared with A17
275 neurons in mammalian retina, the synaptic alignment of APL neurons was slightly less mixed
276 (Fig. S7).

277 Another parameter we applied is the distance between synapses (Fig. S8). For each synapse,
278 the shortest distance to the nearest synapses was identified and recorded. Similarly, the shortest
279 distance between two input synapses was identified in the "input-input" group, the shortest dis-
280 tance between two output synapses was identified in the "output-output" group, and the shortest
281 distance between an input synapse and output synapse was identified in the "input-output" group.
282 Comparing these three sets of data, we found no significant differences in the distribution of the
283 distances, with all being approximately 2 μm. This lack of a difference among these dataset fur-
284 ther describes the mixed arrangement of the synapses; if input and output synapses were separat-
285 ed from each other, the distance in the input-output group would be significantly greater than that
286 in the input-input and output-output groups. Therefore, we conclude that the input and output
287 synapses in APL neurons are arranged in a mixed manner.

288 Importantly, electrical transduction properties differ between thin and enlarged neurites, ac-
289 cording to a previous study (Grimes, Zhang, Graydon, Kachar, & Diamond, 2010; Rall, 1969),
290 with relatively thin neurites exhibiting low conductance. Therefore, the alternating thin and en-
291 larged neurite segments result in a separation of the neuronal activity. Thus is the electrically
292 signal separation basis on Amacrine A17 neurons which have broad branches with varicosities
293 and thin neurites alternate arranged on it, and feedback inhibition to presynaptic biopolar cells

294 located at the varicosities. Thus, APL neurites receive input at enlarged sections and provide
295 output from thin sections, thus constructing a basic local neural circuit unit. Furthermore, APL
296 neurons formed reciprocal connections with neighboring neurons (Fig. 2E), but the identity of
297 these connections neurons required further exploration.
298
299 ***APL neurons mediate the lateral inhibition of KCs in the vertical lobe and the recurrent net-***
300 ***work between APL and KCs***
301 Together with APL neurons, six subtype of KCs, several dopamine neurons, some MBONs
302 and DPM neurons project to the mushroom body and the vertical lobes. A study of the dopamine
303 2 receptor, which supports anesthesia-resistant memory, showed that dopamine neurons make
304 synaptic connections with APL neurons via the D2R receptor (Scholz-Kornehl & Schwarzel,
305 2016). Gap junctions exist between APL neurons and DPM neurons (Pitman et al., 2011; Wu et
306 al., 2011). Blocking the output of KCs completely silences APL neuron activity, suggesting a
307 direct or indirect connection between APL neurons and KCs (Kageyama & Meyer, 1987; Lin et
308 al., 2014). These studies under light microscopy to demonstrate that various neurons are con-
309 nected to APL neurons, but EM evidence is still lacking. To deconstruct the neural circuit com-
310 prising APL and other neurons under EM, the other neurons must first be identified.
311 These reconstructed neurons under EM exhibit specific morphologies under light microscopy
312 that separate them from each other. KCs have no branches (Lee, Lee, & Luo, 1999), while other
313 neurons have extensive branches in the vertical lobe (Aso et al., 2014a, 2014b). Hence, neurons
314 connected to APL neurons were classified based on their proportion in vertical lobe and mor-
315 phology. Morphology of APL neurons mainly consider two features, the length of neurites and
316 the number of bifurcations (Fig. 3CD). Neurites belong to KCs if they have no branches in the

317 vertical lobe and are of a length equal to or slightly less than that of the total vertical lobe. The
318 priori probability of KC for these reconstructed neurons is very high, considering that 1300 KC
319 neurons account for more than 90% of them in the vertical leaves. Neurites that have more than
320 one branch belong to dopamine neurons or MBONs. Our classification data showed that only
321 one output neuron and two input neurons had more than one branch, and most KCs had only one
322 connection with APL neurons (Fig. 3C).
323

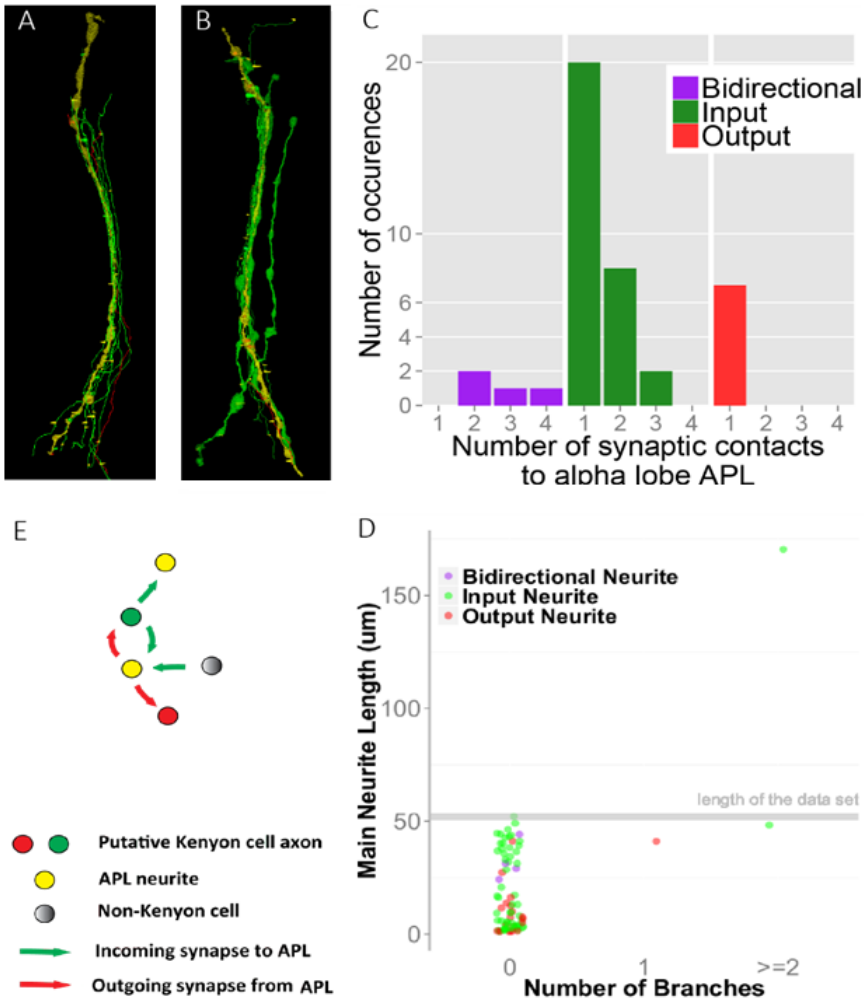

324

325 **Fig. 3. Microcircuit (recurrent network and lateral inhibition) between APL neurons and**
326 **KCs.**

327 **(A)** and **(B)** Two examples of APL input and output neurons. We recognized and traced all of the
328 input and output neurites of APL neurons in the α lobe and the reconstructed 3D structures of
329 some neurites. In this figure, APL neurites are shown in yellow, input APL neurons are shown in
330 green, and APL output neurons are shown in red. The two examples show that these input and
331 output neurons are mostly close to APL neurons; they extend along vertically in a bunch and
332 form synapses with APL neurons, but they separate from the synapses with APL neurons. **(B)** A
333 few reconstructed APL input neurons also have enlarged and thin regions. The APL input syn-
334 apse is represented in green, the APL output synapse is shown in red, and synapses connecting to
335 other neurons are shown in yellow. **(C)** The numbers of synapses connecting APL neurons with
336 input and output neurons. The green bars indicate the distribution of synapses between APL and
337 input neurons. The red bars indicate the distribution of synapses between APL and output neu-
338 rons. The purple bars indicate the distribution of synapses between neurons that have both input
339 and output connections with APL neurons. More than 60% of neurons form single synapses with
340 APL neurons. All input and output neurons had a total length greater than 10 μm. **(D)** All neu-
341 rons connecting to APL neurons are Kenyon-like neurons. The x- and y-axes represent the num-
342 ber and length of the branches, respectively. The morphologies of most input and output neurites
343 contain only one main neurite, i.e., had zero branches. Many neurons with only one main neurite
344 were longer than 25 μm, or even near 50 μm, almost equaling the length of the α lobe in our da-
345 taset (52 μm, gray horizontal line in D). Therefore, these neurons nearly extend across the α lobe
346 and have morphologies similar to those of KCs. One neuron with branches extends across the α
347 lobe with multiple lengths of the α lobe (green point in the upper right corner of D). This obser-
348 vation suggests that multiple types of input neurons connect to APL neurons. Green point: Input
349 neurons of APL neurites. Red point: Output neurons of APL neurites. Purple point: Neurons with

350 input and output connections to APL neurites. **(E)** Microcircuits between APL and KC neurons,
351 including recurrent network and lateral inhibition.

352 We concluded that several circuits exist in the vertical lobes of mushroom bodies between
353 APL neurons and other neurons (Fig. 3E). We found lateral inhibition and a recurrent network
354 between APL neurons and KC neurons in the vertical lobe. This circuit comprising dopamine
355 neurons projecting to KCs constitutes the neural basis for decoding of odor learning, decision
356 making, mutual suppression of relational odor, and reversal learning. EM reconstruction data re-
357 vealed that in the vertical lobe, KC neurons projected to APL neurons non repetitively (Fig.
358 S11). One strategy for fulfilling the function of specific inhibition is utilizing the local microcir-
359 cuit between APL neurites and KCs at different compartmental parts with dopamine neurons.
360 Therefore, KC axons may be compartmentally modulated by not only dopamine but also APL
361 neurons.

362

363 ***APL neurons generate no action potential***

364 Amacrine A17 neurons in which multiple independent microcircuits exist in a single neuron
365 (Grimes et al., 2010), are nonspike and axon-less neurons. Small axon-less neocortical interneu-
366 rons, which are also nonspike neurons, communicate with each other through dendrodendritic
367 local circuits (le Magueresse et al., 2011). Neurons generating no action potential send signals
368 via graded membrane potential to form microcircuits, whereas neurons generating action poten-
369 tials function as a single unit; therefore, local circuit is easily formed by non spike neurons but
370 not spike neurons. Other dendrodendritic microcircuits exist between excitatory mitral cells and
371 inhibitory granule cells (Osinski & Kay, 2016). GGNs (the homolog of APL neurons) in locusts
372 normalize the KC odor response via global inhibition, generating no action potentials to odor

373 stimuli (Papadopoulou et al., 2011). Therefore, we examined this electrophysiological property
374 of APL neurons. We depolarized the cell bodies of APL neurons (n=5) with a slope from -30 mV
375 to 80 mV, and none of the APL neurons elicited an action potential (Fig. S12). Such, APL neu-
376 rons are similar to the axonless amcrine A17 neurons and neocortical interneurons. Moreover,
377 we examined whether electrical stimuli are transferred from APL cell bodies to lobes. Indeed, we
378 failed to record changes in the voltage signal in the lobes upon depolarization of cell bodies.
379

380 ***APL neurites in the α and α′ lobe respond to odors independently***

381 First, we tested whether APL neurons in the α and α′ lobes function independently. The recon-
382 structed EM data showed only one neurite connecting the α and α′ lobes in the vertical lobe (Fig.
383 1FG). The structural separation between the α and α′ lobes of APL neurites indicates that these
384 lobes might function independently based on their local circuitry with KCs in α and α′ lobes sep-
385 arately. Moreover, octopaminergic APL neurites in the α lobe have been shown to maintain anes-
386 thesia-sensitive memory, while APL neurites in the α′ lobe facilitate visual reversal learning; this
387 functional separation of the APL – KC at α and α′ lobes circuit is consistent with our hypothesis.
388 Previous studies found that APL neurons depolarize in response to both odors and electrical
389 stimuli (Liu & Davis, 2009; Wu et al., 2011). APL neurons in the vertical lobe can also respond
390 to odors (Lin et al., 2014). Thus, the different responses property of APL neurons in the α and α′
391 lobes to odor and electrical stimuli were explored.
392 To test our hypothesis that APL neurons have independent local circuits in the α and α′ lobes,
393 we used dual-color calcium imaging to observe the responses of APL neurons and mushroom
394 bodies, *GH146-Gal4/UAS-GCaMP6s; 247-LexA/LexAop-R-GECO* (Fig. 4E). Overall, angular
395 distance data showed that the APL neurites responded to odors more generally than did the KCs.

396 These data are consistent with previous research results (Wu et al., 2011). And, APL neurites in
397 the α lobe and α′ lobes were shown to respond to odors differently. Firstly, the maximal APL
398 peak response in the α lobe was much larger than that in the α′ lobe (Fig. 4AB). Additionally,
399 among all of the responsive regions of interest (ROIs), APL neurite at the α lobe tended to re-
400 spond to more odors than that at the α′ lobe (Fig. 4CD), while they have better odor separation of
401 APL neurite in α′ lobe than in α lobe (Fig. 4EFG). Second, both ON and OFF responses were
402 observed in APL neurites, especially those in the α lobe, which exhibited a greater OFF re-
403 sponse, suggesting that KCs have not only ON responses (Li, Li, Lei, Wang, & Guo, 2013) but
404 also OFF responses. Thus, APL neurites in the α and α′ lobes respond to odors differently and
405 independently. This difference might be due to different input KC response properties in the α
406 and α′ lobes.

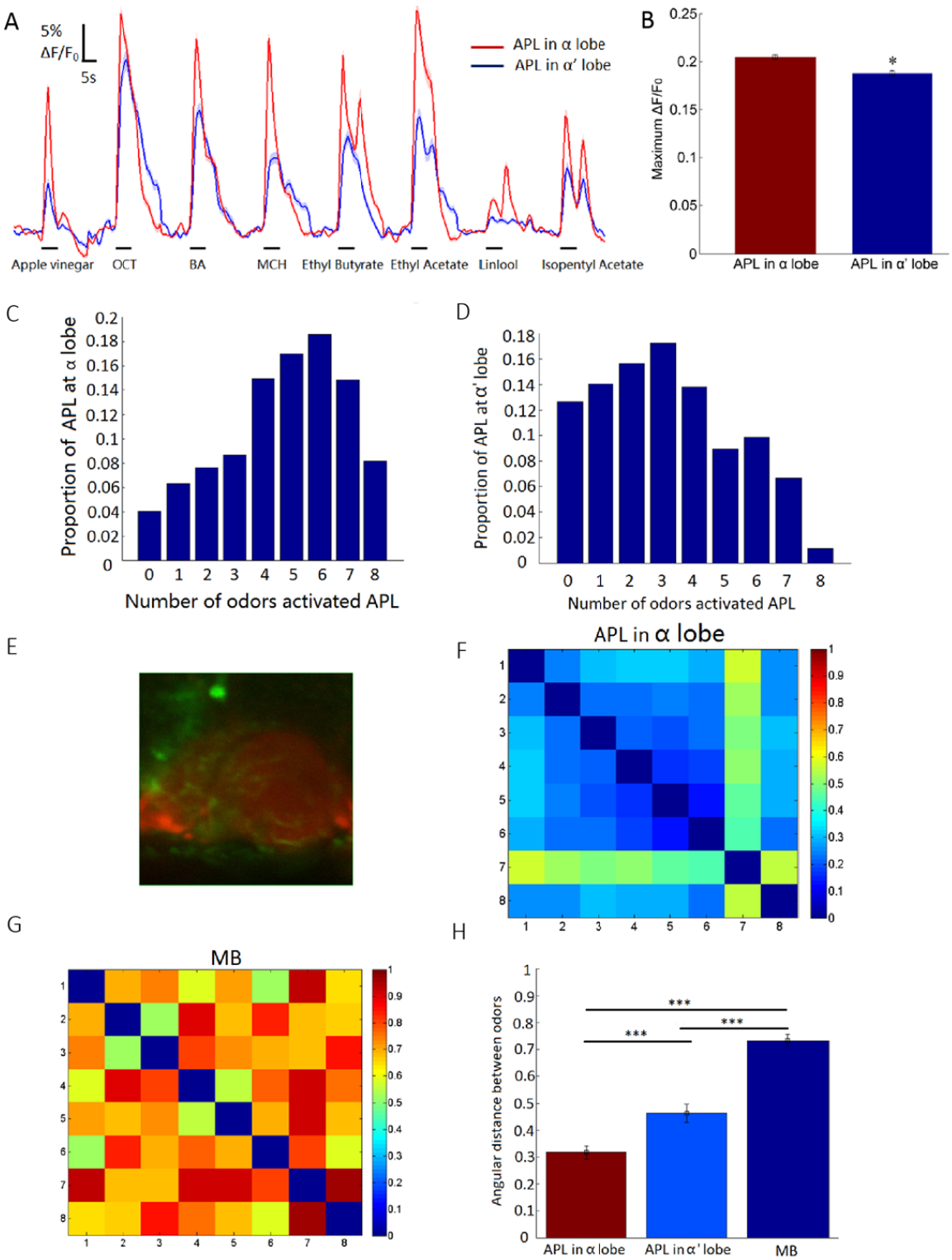

Fig. 4. APL neurons in the α and α′ lobes respond to odors differently

409 **(A)** Mean curves of APL responses to eight odors showing that the peak response of the α lobe is
410 larger than that of the α′ lobe. Odors delivered to the flies included apple vinegar, OCT, BA,
411 MCH, ethyl butyrate, ethyl acetate, linalool, and isopentyl acetate. **(B)** The peak responses of
412 APL neurites in the α lobe are larger than those in the α′ lobe (Wilcoxon rank-sum test, $P < 0.05$,
413 $P = 8.947\times10^{-6}$). **(C)** APL neurites in the α lobe responded to more odor types. **(D)** APL neurites
414 in the α′ lobe responded to fewer odor types. In (A) and (B), the horizontal axis represents the
415 number of responsive odors, and the vertical axis represents the percentage of responsive ROIs.
416 **(E)** Horizontal map of an APL and mushroom body in the vertical lobe by dual-color calcium
417 imaging. The fly genotype is *GH146-Gal4/UAS-GCaMP6s; 247-LexA/LexAop-R-GECO*, n = 10.
418 **(F)** Angular distance heatmap of APL neurites in the α lobe responding to eight types of odors
419 demonstrating that APL neurites separate odors poorly. **(G)** Angular distance heatmap of a
420 mushroom body responding to eight odors demonstrating that mushroom bodies can separate
421 odors well. **(H)** Mean angular distances of mushroom body and APL responses to different odors
422 showing that mushroom bodies can separate odors better than APL neurites, while APL neurites
423 in the α′ lobe separate odors better than those in the α lobe (Wilcoxon rank-sum test, $P < 0.001$. P
424 (α & α′) = 0.0013, P (α & MB) = 4.59×10^{-17}, P (α′ & MB) = 4.37×10^{-8}).
425
426 ***Odor evokes a local calcium microdomain on a single APL neurite***
427 The calcium signal has been shown to be a good indicator of neuronal activity, especially after
428 the advent of GCaMP6 (Chen et al., 2013). We used a single APL fiber calcium imaging method
429 to observe its calcium signal for different odors (Single neurite imaging, Fig. S13). The alternate
430 arranged enlarged and thin sections of the APL neurites enables the different electrical conduct-
431 ance across the neurite (Rall, 1969). This suggests that a separate calcium activity zone can be

432 seen on the nerve fibers. Secondly, blocking KC output completely abolished the responses of
433 APL neurons to odors physiologically (Lin et al., 2014). Besides, KC codes odor sparsely and
434 separate odor well, only a few KCs respond to more than one odors (Lei et al., 2013). Structural-
435 ly EM reconstruction data revealed that in the vertical lobe, KC neurons projected to APL neu-
436 rons nonrepetitively (Fig. S11); Thus, local circuits between APL neurons and KCs enabled the
437 differential and local calcium response of APL neurite to odors.

438 Therefore, to address whether odors can induce local and different calcium responses in APL
439 neurons, we observed single APL neurite calcium activity at the vertical lobe via expressing
440 GCaMP6 driven by *APL-GAL4*. APL neurites are imaged across layers from top to bottom and
441 then we compared single neurite activities within the same layers, found local calcium microdo-
442 mains on APL neurites induced by different odor inputs (Fig. 5A). Local calcium domains have
443 been demonstrated to be electrically separated from each other on a neurite (Goldberg, Gabor,
444 Dmitriy, & Rafael, 2003). The imaged APL neurites were classified into three categories: neu-
445 rites that responded to all odors locally (46%), those that locally responded to some of the eight
446 odors (34%), and those that did not respond to any odors (20%) (Fig. 5ABC) (Table 2). That
447 might due to different APL neurons receive different KCs input at different location. Some KCs
448 could respond to more than one odor, while other KCs code non odor information but tempera-
449 ture and others. These phenomenon were consistent with our hypothesis. Another explanation for
450 the local calcium domains could be an uneven calcium channel distribution. To exclude this pos-
451 sibility, we delivered electrical and odor stimuli separately to Drosophila. The responses to elec-
452 trical and odor stimuli are first mediated by different neurons; the response to electrical stimuli is
453 primarily mediated by dopamine neurons (Claridge-Chang et al., 2009; Mao & Davis, 2009),
454 which then transfer the information to APL neurons directly or indirectly via KC neurons. In

455 contrast, the response to odor stimuli is mediated by KCs. Second, KC neurons project to APL at
456 different locations. If localized APL neuron responses are due to different inputs and not to an
457 uneven calcium channel distribution, then APL neurons should respond to odors differently
458 when exposed to different stimuli. The inability of these neurons to respond to odor signals acti-
459 vated by an electrical stimulus demonstrates that they are activated by different inputs in differ-
460 ent regions. Thus, APL neurites displayed local input-dependent output activity but not a global
461 output signal (Fig. 5D). 3D reconstruction of volume calcium imaging APL neurites via tracing
462 mCherry expression in the vertical lobe showed local calcium responses from the top to the bot-
463 tom of the lobe (Fig. 5E). Additionally, responses of the same neurites across several layers
464 demonstrated significant local responses to odors (Fig. 5F). These local calcium domains suggest
465 poor propagation of the calcium signal along the APL neurite. This local calcium response prop-
466 erty is common on divided leaves of the vertical lobe (Fig. 5G). We also calculated the prefer-
467 ence of odors in different APL neurites, which displayed a different preference but not an even
468 response (Fig. S14).
469
470 **Table 2 Statistical data of various APL neurite responses to odors**

Kinds of APL neurite responses to 8 odors	Proportion
Local response to 8 odors	47/103 (46%)
Non response to odors	21/103 (20%)
Local response to part odors	35/103 (34%)

471

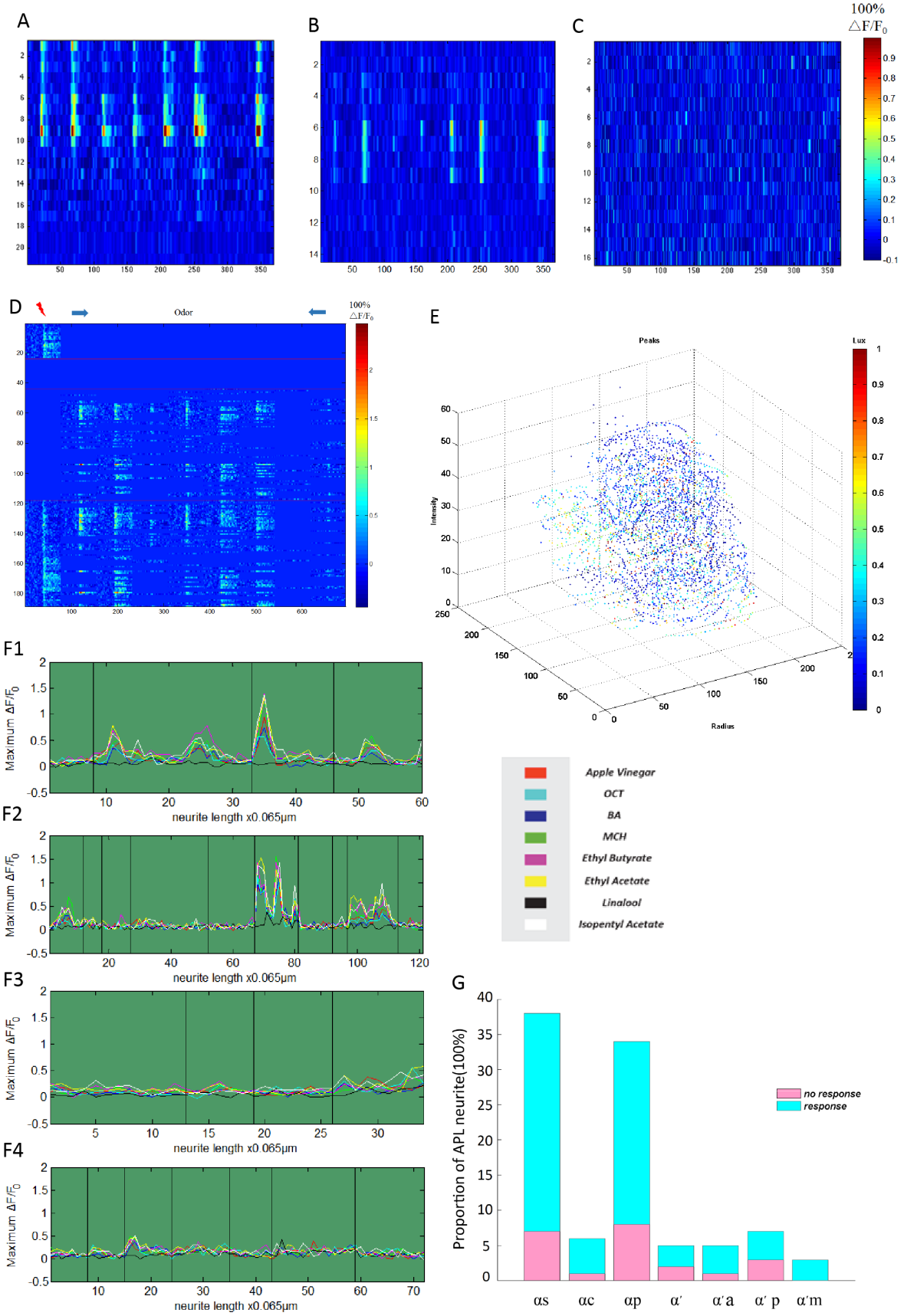
A
B
C
100%
△F/F0
D
Odor
E
Peaks
Lux
Intensity
Radius
F1
F2
F3
F4
Maximum ΔF/F0
neurite length x0.065μm
Apple Vinegar
OCT
BA
MCH
Ethyl Butyrate
Ethyl Acetate
Linalool
Isopentyl Acetate
G
Proportion of APL neurite(100%)
no response
response
αs
αc
αp
α′
α′a
α′ p
α′m

472

473 **Fig. 5. Localized calcium domain on a single APL neurite**

474 **(A)**. APL neurites that respond to some odors (odor stimulus label is the same as in Fig. S13). **(B)**
475 APL neurites that respond to all odors. **(C)** APL neurites that respond to no odors. In (A), (B)
476 and (C), the vertical axis represents the length of neurites, the horizontal axis represents the time
477 of calcium imaging with odor stimuli, and the heat value represents the peak responses to odors.
478 Eight different odors were delivered in the sequence listed in Fig. 4A for each heatmap. *GH146-*
479 *Gal4/UAS-GCaMP6s; UAS-mCherry/+*, n = 5. **(D)** Electrical stimuli activated different APL
480 neurites than odor stimuli. The first area represents APL neurites activated by only electrical
481 stimuli. The second area represents APL neurites that did not respond to either odor stimuli or
482 electrical stimuli. The third area represents APL neurites that only responded to odor stimuli. The
483 fourth area represents APL neurites responded to both odor stimuli and electrical stimuli. The red
484 lightning bolt represents a 60 V electrical stimulus applied for 5 s. Eight different odors are
485 shown in Fig. 4A. *GH146-Gal4/UAS-GCaMP6s; UAS-mCherry/+*, n = 3, n (ROI) = 190. **(E)**
486 Local peak responses to apple vinegar in the 3D structural representation of APL neurites. The x-
487 and y-axes represent the horizontal level, the z-axis represents the vertical level, and the light
488 intensity represents the response intensity at that point. **(F)** The same APL neurite across differ-
489 ent layers demonstrating a localized response property to odors. F1-F4 represent four different
490 APL neurites. The horizontal axis represents the length of APL neurites across different layers.
491 Each black line represents the joint between two neurites at different layers belonging to the
492 same neurite. The vertical axis represents the peak response of calcium imaging to odors.
493 *GH146-Gal4/UAS-GCaMP6s; UAS-mCherry/+*, n = 4. **(G)** APL neurites in different subareas of
494 the mushroom body vertical lobe, all displaying the local response property. The horizontal axis

495 represents APL neurites in different subareas of the mushroom body, and the vertical axis repre-
496 sents the percentage of responding (blue bar) and nonresponding APL neurites (pink bar).
497
498 ***APL neurites send out signals locally both in the calyx and the vertical lobe depending on***
499 ***odor stimuli***
500 Because APL neurites respond to odors locally depending on the local input in the vertical lobe,
501 we examined whether they also send out signals locally in the calyx and vertical lobe, since the
502 same local circuits are present in both the calyx (*unpublished*) and vertical lobe. We expressed a
503 presynaptic-specific calcium indicator, syt-R-GECO, driven by *GH146-Gal4* and *APL-Gal4* and
504 then observed APL output signal responses to 8 different odors in the vertical lobes (Fig. 6A)
505 and calyx. Heatmaps of APL neuron presynaptic calcium activity signals displayed local odor
506 dependent activity in both the vertical lobe and calyx (Fig. 6BC).
507
508

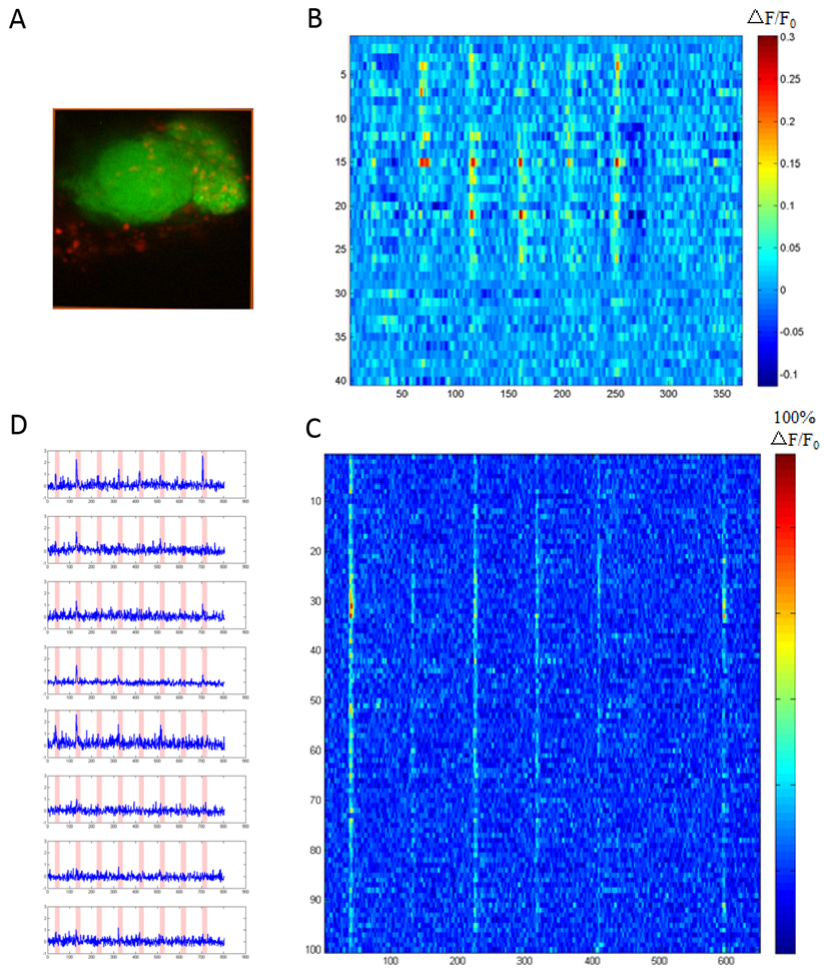

Fig. 6. Localized responses of an APL presynaptic calcium indicator to odors.

(A) Distribution of presynaptic APL neuron proteins in the mushroom body vertical lobe. *GH146-Gal4/+; UAS-syt-R-GECO/247-LexA-LexAop-GCaMP6s*, n = 7, n (ROI = 40). The green area represents labeled KCs, and the red area represents presynaptic proteins in APL neurons. **(B)** Local responses of an APL presynaptic calcium indicator to eight odors in the mushroom body vertical lobe. **(C)** Local responses of an APL presynaptic calcium indicator to eight odors in the mushroom body calyx. **(D)** Eight ROIs of APL-localized presynaptic site responses to 8 different odors in the calyx. (C and D) *UAS-syt-R-GECO/+; APL-Gal4/+*, n = 3, n (ROI) = 100. (BCD). Odor stimuli are the same as mentioned in Fig. 4A.

In the calyx, regions of APL neurites labeled by presynaptic proteins responded broadly to the first odor, providing structural evidence of global APL neurite distribution (Fig. 6C). In contrast, only some presynaptic protein-labeled APL neurite regions responded to other odors, and the activated presynaptic APL neurite areas differed among odors, demonstrating that APL neurites show local but not global odor-dependent activity. Examples of a single presynaptic calcium unit displaying odor-specific local presynaptic activity are shown in Fig. 6D.

Previous studies found that GABAergic neurons project to KC dendrites and projection neuron axons in the calyx (Yasuyama, Meinertzhagen, & Schurmann, 2002), implying that a feed-forward inhibitory circuit between APL neurons and projection neurons may exist in the calyx (Olsen & Wilson, 2008). Whether KCs or projection neurons project to APL neurons in the calyx, forming local neural circuits with APL neurons, requires further study.

In summary, the evidence presented support the presence of a local recurrent circuit of APL neurons and KCs in the vertical lobe (Fig. 7).

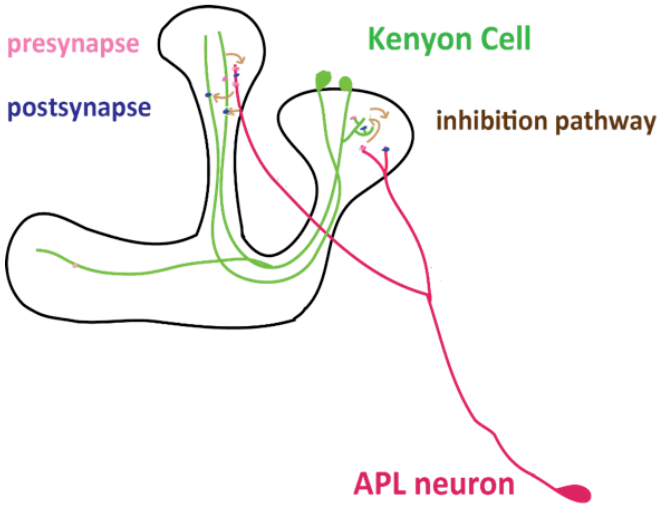

534 **Fig. 7. Working model of the circuit between APL neurons and KCs.**

535 Mutual and local inhibition circuits between APL neurons and KCs in the mushroom body verti-
536 cal lobe. We hypothesize that local circuits exist in the mushroom body calyx. The green curves
537 represent KCs, and the red curves represent APL cells. Connection circuits that potentially exist
538 between other neurons and APL cells are not shown.

539

540 **Discussion**

541 Mushroom body and APL neurons play important roles not only in learning and memory but also
542 in high cognitive behavior, reversal learning, learning, and decision making (*unpublished*). The
543 circuit of APL and KCs in the mushroom body underlies this behavior in reversal learning. To
544 reveal the specific circuits that have remained unknown, we applied series continuous EM meth-
545 ods. Here, we reconstructed the connections between the mushroom body and APL neurons in
546 the vertical lobe of the mushroom body via FIB-SEM and genetic labeling of APL neurons with
547 HRP. We found recurrent network and lateral inhibition connections between APL neurons and
548 KCs in the vertical lobe of the mushroom body. Reconstruction of the mushroom body in *Dro-*
549 *sophila* larva also found APL-KC recurrent networks (Eichler et al., 2017), which are the neural
550 basis underlying high cognitive behavior. Other reconstruction neural circuit work in the calyx of
551 the mushroom body also revealed a recurrent network between the APL neurons and KCs
552 (Zheng et al., 2018). Moreover, while dopamine neurons projecting to mushroom body axons
553 result in local KCs function, APL neurons receive input from KCs and also well intermixed with
554 mushroom body compartmental structure, whether APL neurons function locally remained un-
555 certain. APL neurons exhibited intermixed presynapses and postsynapses in both the calyx and
556 vertical lobe. We thus used EM reconstruction, electrophysiology and calcium imaging methods

557 to explore the local function of APL neurons. In the vertical lobe, APL neurites resembled a
558 string of beads with input synapses and output synapses intermixed on enlarged and thin sections
559 of the neurite. KCs were found to project to APL neurons nonrepetitively (Fig. S11), forming a
560 local circuit. Furthermore, using a single neurite calcium imaging method, we found that local
561 calcium domains enabled electrical separation of the APL neurite. APL neurons were found to
562 send odor-dependent signals in a local but not global manner not only at calyx but also at lobe.
563 Furthermore, the vertical lobe was shown to have odor-dependent properties but not global prop-
564 erties. At the vertical lobe, APL neurites only formed connections with 2/3 KC neurons, which is
565 insufficient for a global inhibition network. Consistent with the functional separation of the α
566 lobe and α′ lobe in anesthesia-sensitive memory, Reconstructed APL neurons exhibited a separa-
567 tion at these lobes and APL neurons exhibited independent responses to odors in these lobes.
568 These findings support the hypothesis that APL neurons function locally.

569 To reconstruct brain circuits on the nano scale, two strategies in volume reconstruction have
570 been applied till now: one is dense reconstruction of all neurons in a specific area and the other is
571 sparse reconstruction, reconstruction of sparsely labeled neurons and their connected neurons.
572 The mushroom body of *Drosophila* larva (Eichler et al., 2017), the calyx of adult *Drosophila*
573 (Zheng et al., 2018), and the entire brain structure of *C elegans* (Cook et al., 2019) have been
574 reconstructed using the first method. The second method has been pioneerly applied in our work.
575 Due to its specific labeling, the second method takes priority in dramatically less time and labor
576 consumption of data acquisition, analysis and data storage than the first one. Since the first one
577 needs to get the whole brain EM data, and then focus on specific region to reconstruct all com-
578 plete neuron structure, the second one only get the specific brain EM data and reconstruct the
579 labeled neurons and its connection neurons. Due to these conveniences and accuracy of sparse

580 reconstruction, reconstruction work of specific interesting brain area neuron circuits with few
581 group of people could realize and be valuable. To approach this aim, we have first overcomed
582 the technique challenge of specific labelled EM sample preparation, continuous labeled neurons
583 and better image contrast. The HRP labeled method, which limitation is relative small neural
584 network boundary, is more reliable and highly permeable in all published methods (Larsen, 2003;
585 Shu et al., 2011) after we tested. Besides, in more specific brain area EM acquisition of Drosoph-
586 ila and C elegans, higher precision imaging method dual beam series scan electron microscopy
587 (FIBSEM) (Heymann et al., 2006; Knott, Marchman, Wall, & Lich, 2008), which gives much
588 more reliable EM data because its thinnest imaging layer than serial section TEM (ssTEM)
589 (Zheng et al., 2018), serial scanning TEM (ssTEM) (Briggman & Bock, 2012), automated tap-
590 collecting ultramicrotome SEM (ATUIM-SEM) ((Hayworth, Kasthuri, Schalek, & Lichtman,
591 2006) and serial block-face SEM (SBSEM) (Denk & Horstmann, 2004) is applied.

592 APL neurons and mushroom bodies play important roles in highly cognitive behavior, includ-
593 ing visual reversal learning, olfactory reversal learning and visual decision making. Direct evi-
594 dence suggests that the connection between APL neurons and KCs participates in the reversal
595 learning behavior of *Drosophila* (Wu et al., 2012). However, the specific neural circuit between
596 APL and KC neurons has remained undiscovered. Our EM work in the vertical lobe of the mush-
597 room body identified two main circuits: a recurrent network and a lateral inhibition circuit. They
598 might underlie these behaviors. Furthermore, simulation work on recurrent networks has demon-
599 strated that these networks are able to facilitate a winner-take-all neuronal signaling process in
600 limited amounts of time (Liu, Dang, & Cao, 2010) and will quickly realize adaptive orthogonal
601 filters and associative memory (Kohonen & Oja, 1976). Indeed, recurrent networks in the cortex
602 are important in action selection (Haga & Fukai, 2018), decision making (Wang, 2008; Wong,

603 2006), learning (Gianluigi, Amit, & Nicolas, 2003) and reversal learning processes. The mush-
604 room body of *Drosophila* and the cortex of mammals have been suggested to be evolutionarily
605 identical (Tomer, Denes, Tessmar-Raible, & Arendt, 2010). Thus, the recurrent network identi-
606 fied here may be evolutionarily conserved.

607 APL neurons in the vertical lobe of the mushroom body display local activity to odor stimuli.
608 Previous work showed that APL neurites might not have strict local circuits; upon selective
609 blockade of different KC subtypes, there were no significant increases in the responses of the
610 corresponding KCs (Lin et al., 2014). This phenomenon could also be explained by the existence
611 of a connection between different KC subtypes, potentially compensating for the effect of block-
612 ing a single KC subtype. Indeed, recent studies have identified a gap junction between different
613 KC subtypes, but whether a chemical connection exists between different KC subtypes remains
614 to be explored. Therefore, local APL circuitry could also exist under this condition. Another pos-
615 sibility is that DPM neurons in different lobes might be well connected such that even if one KC
616 subtype is blocked, DPM neurons connected with other subtypes might compensate for this ef-
617 fect due to their ability to elicit the release of acetylcholine from KCs via gap junctions between
618 APL and DPM neurons. However, more experimental evidence is needed to support this possi-
619 bility. The third possibility is that extrinsic inhibitory interneurons may broadly receive input
620 from KC axons and deliver output to APL neurons. Another work showed that APL neuron ac-
621 tivity was global or specific depending on the olfactory input strength to the mushroom body
622 (Inada, Tsuchimoto, & Kazama, 2017). In the calyx, partial activation of projection neurons in-
623 duces partial KC inhibition, which arises from the local but not global activity of APL neurons.
624 This finding is consistent with our finding in the calyx. The calcium response of APL neurons
625 throughout the horizontal lobe was found to increase in response to increasing odor concentra-

626 tion gradients. Increased odor concentration will increase KCs response, which induce high APL
627 response property, it does not mean that the response is global. First, the increase in the APL
628 neuron response cannot exclude the possibility of a DPM neuron electrical coupling effect
629 (Pitman et al., 2011; Wu et al., 2011). More importantly, the difference in research methods
630 used, such as whole-area imaging versus single neurite imaging, might have led to different con-
631 clusions. The single neurite calcium imaging method used here provides a more precise signal
632 than the previous method. Another possible explanation is that APL neurites in the horizontal
633 lobe might function differently from those in the vertical lobe.

634 Local circuits between APL neurons and KCs in the vertical lobe function in compartmental
635 functional mushroom body structures. Mushroom bodies contain 15 independent compartmental
636 function structures separated by locally projecting dopamine and extrinsic neurons. This func-
637 tional compartmentalization increases the computation capacity of mushroom bodies (Aso et al.,
638 2014a), and familiar strategies are applied by amacrine A17 neurons (Grimes et al., 2010).
639 Broadly innervated APL neurons also work locally, which is another strategy to increase the
640 computational complexity in a limited space. The local circuits in APL neurons act together with
641 the compartmental structures of mushroom bodies and facilitate different mushroom body area
642 responses, and similar local circuits have been identified in amacrine A17 neurons. Additionally,
643 our data suggest that APL neurons exhibit segmental plasticity, which is also supported by evi-
644 dence that APL neurons specifically respond to learned odors (Liu & Davis, 2009). The distance
645 between local circuits in APL neurons and whether these circuits are restricted to thin and en-
646 larged regions, or even beyond these regions, remains unanswered. This question needs to be fur-
647 ther studied by depolarizing a single APL neuron input and then observing the distance of signal
648 propagation (Grimes et al., 2010). This technology is difficult to realize due to the fleeting calci-

649 um signal on a single neurite. More questions including what's the relationship of APL local
650 neurons and DA-MBON-KC compartmental structure also remains to be further study. And
651 what's the contribution of APL and DA separately on local KC signal.

652 Another circuit found between APL neurons and KCs is a lateral inhibition circuit. Lateral in-
653 hibition between APL and KCs increases the signal contrast. The circuits might not only mediate
654 competition between different types of odor information but also other sensory information in
655 mushroom bodies, as mushroom body KCs encode not only olfactory information but also visual
656 information, taste (Kirkhart & Scott, 2015) and temperature (Frank, Jouandet, Kearney,
657 Macpherson, & Gallio, 2015). However, to complete understand the whole circuit function, the
658 identity and role of other neurons connected with APL neurons remains to be explored in future
659 work. As mentioned previously, dopamine neurons form dopaminergic connections with APL
660 neurons. Together, dopamine neurons (Ke, Guo, Peng, Wang, & Aike, 2007), KCs and APL neu-
661 rons form the salience-based decision-making circuit (Guo, Zhang, Ren, Su, & Chen, 2016). The
662 specific circuit remains unexplored, and its identification may enhance our understanding of de-
663 cision-making processes. Dopamine may also act with APL neurons and KCs to effect reversal
664 learning behavior. Here, dopamine encodes value information about KCs, and MBONs encode
665 the decision-making behavioral output? Additionally, the 15 functionally distinct compartments
666 of mushroom bodies are suggested to form a multilayered feedforward learning module in which
667 dopamine encodes reward and APL neurons encode punishment. However, the specific circuit
668 for this coding and computing behavior requires more detailed information (Aso et al., 2014a).
669 Finally, whether decision-making circuits also include different compartmental parts of the
670 mushroom body remains to be explored.

671

672 **Methods**

673 ***Fly strains***

674 The flies used in this experiment were as follows: *APL-GAL4* (Ann-Shyn Chiang), *GH146-*
675 *Gal4* (Tanaka et al., 2008), *247-LexA*, *UAS-HRP-mCD8-GFP* (Jean-Paul Vincent), *UAS-*
676 *GCaMP6s*, *UAS-syt-R-GECO (unpublished)*, *LexAop-GCaMP6s*, *UAS-synaptobrevin-GFP*
677 (Bhattacharya et al., 2002), *UAS-mGFP*, *UAS-n-synaptobrevin-GFP* and *UAS-mCherry*. All flies
678 were raised in an incubator at a constant temperature and humidity of 25°C and 50%, respective-
679 ly, with a 12 h dark/12 h light circle. The flies were supplied Bloomington standard food, and
680 crossed flies were collected as virgins for calcium imaging experiments.

681

682 ***EM tissue preparation***

683 Three-day-old male *GH146-Gal4>UAS-HRP-mCD8-GFP* flies were used for EM preparation.
684 The *Drosophila* brains were dissected according to custom procedures. Fixation was performed
685 to ensure that the *Drosophila* brains were HRP-positive under a light microscope. The brains
686 were fixed in glutaraldehyde for 30 min at 25°C, dyed with HRP, and then washed with 0.1 M
687 PB three times for 5 min each time and incubated with TSA biotin for 16 h at 4°C. Then, the
688 brains were washed and incubated with ABC for 16 h at 4°C. The brains were then washed with
689 Tris-HCl, incubated with DAB first at 4°C for 30 min and then at 25°C for 15 min, and washed
690 with 0.1 M PB. For EM sample preparation, the brains were fixed with prechilled 2% OsO4 PB
691 for 2 h at 4°C, washed with ddH2O, dyed with 2% uranyl acetate for 20 h at 4°C, washed with
692 ddH2O, and then pre-embedded in 1% agarose at 42°C. After the agarose set, it was trimmed
693 into a trapezoid. Dehydration and resin impregnation were performed according to the standard
694 EM method. Fly brain resins embedded in agarose were dried in an incubator at 37°C for 12 h,

695 42°C for 12 h and 60°C for 48 h. The resins were carefully trimmed to expose the vertical lobe
696 of the mushroom body for dual beam electron microscope imaging.
697
698 ***EM data imaging and reconstruction procedures***
699 *Imaging data capture parameters and results*
700 We performed carbon plating for the EM samples and glued them to the EM sample plate. We
701 then placed an EM sample with plates inside the dual beam scanning electron microscope (Heli-
702 os Nano Laboratory 600i, FEI). A 1.5-μm-thick layer of platinum was placed onto the surface
703 perpendicular to the block face to be imaged. A focused electron beam was used to image the
704 block face after the focused ion beam was used to remove a 40-nm-thick block face and expose a
705 new one to be imaged. These two steps were repeated until the entire dataset was finished. Plati-
706 num plating and imaging capture were performed using AutoSlice & View^{TM} software (FEI). In
707 total, 1300 images were acquired, and every image pixel was 4096×4096 with a pixel distance of
708 7 nm.
709
710 *Reconstruction procedure (neurite reconstruction: node, line, 3D reconstruction)*
711 All images were aligned in FIJI TrackEM2 by SIFT alignment. Due to the lower accuracy of
712 autosegmentation of neurites, manual labor was preferred. Approximately 5-6 annotators sepa-
713 rately identified darkened neurites and synapses in each layer and then cooperated to proofread
714 and vote on the merged results according to a strict standard. Only nodes or synapses more than
715 80% positive were subjected to a recheck, and only 100% positive data were accepted to ensure
716 the authenticity of the dataset. Additionally, the missed data (non-100% positive data) were add-
717 ed in the next analysis procedure. Then, the results from all of the annotators were merged for

718 further analyses. The overall marking/proofreading-voting-merging cycle was repeated with the
719 help of modified TrackEM2. In all analyses, all neurons and synapses were checked at least 3
720 times, and several areas were checked 5 times. In the end, we are confident that we obtained
721 100% correct data. In addition, based on this process, we annotated APL neurite skeletons, APL
722 synapses, input neuron skeletons, input neuron synapses, output neuron skeletons and output
723 neuron synapses one-by-one. To obtain volume data for some neurites, we performed neurite
724 segmentation by a semiautomatic method (*Supplemental material)*.
725
726 *Neurite radius extraction and data analysis*
727 Neurite radius computation was based on 3D neurite data. The minimum section area (A) of a
728 neurite at a specific node was calculated, and the radius of a specific node was calculated as the
729 radius of a minimum section area. Thus, $r=\sqrt{A/\pi}$. The code for neurite radius computation was
730 written using Python (v2.7, www.python.org), and the results were saved as xml files. All other
731 data were acquired by running scripts in FIJI via the TrackEM2 program interface. We then ana-
732 lyze these data in R and plotted the data via ggplot2. The data were modified, and the typeset
733 figures were created using an illustrator (Adobe Systems Inc.).
734
735 **In vivo *calcium imaging***
736 *Odor delivery*
737 Eight different odorants, 4-methylcyclohexanol (MCH), octanol (oct), butyl acrylate (BA),
738 apple vinegar, ethyl butyrate, ethyl acetate, linalool, and isopentyl acetate, were separately dilut-
739 ed in mineral oil at a ratio of 1:100. All odorants were purchased from Sigma at the highest puri-
740 ty possible. The odorants were pumped into the fly chamber at a final speed of 400 ml/min via a

741 pipe (microdiaphragm pump, model HC400DC). The ventilated pipe was placed 1 cm from the
742 fly antenna. The time (5 s) and interval (18 s) of odor delivery were controlled using MATLAB
743 software. The odor delivery timing accuracy was adjusted using a photoionization detector (min-
744 iPID, Aurora Scientific Inc.). All of the above odorants were purchased from Sigma-Aldrich at
745 the highest purity possible.
746
747 *Electrical stimuli*
748 Flies were prepared as mentioned before for in vivo calcium imaging. Then, the fly was placed
749 in a chamber with copper on it, which was connected to electrical power, ensuring that their ab-
750 domens and legs touched the copper. The time and duration of electrical stimuli were controlled
751 by MATLAB software. Finally, 60 V of electrical power was delivered to the fly for 5 s.
752
753 *Calcium imaging*
754 Flies expressing *UAS-GCaMP6s* via *GH146-Gal4* were anesthetized on ice and then trans-
755 ferred to 4°C. They were then placed on a classic imaging plate with their antenna beneath the
756 plate. The point at which the fly and plate connected was covered with ultraviolet glue (UV 353
757 Loctite) and then fixed with an ultraviolet lamp for 20 s. The head cuticle between the two eyes,
758 fat body and trachea were carefully removed with fine forceps. The fly brain was immersed in
759 extracellular solution for cells (ESC) (Wilson, Turner, & Laurent, 2004). The plate was then re-
760 versed, and the proboscis cuticle was cut to ensure that the skeleton was bendable and stable. The
761 reversed plate was then placed under a NIKON FN1 microscope with a Nikon Apo LDW
762 25x/1.1w water objective. The excitation wavelength was 488 nm. We acquired images with

763 256×256 pixels at a speed of 8 Hz. For multiple-layer imaging, each step was 4 μm. The setup
764 for the experiment, including odor stimuli and electric stimuli, is shown in Fig. S15**.**
765 Dual-color flies containing *GH146-Gal4/UAS-syt-R-GECO*; *247-LexA-LexAopGCaMP6s*
766 and *GH146-Gal4/UAS-GCaMP6s*; *UAS-mCherry/+* and *GH146-Gal4/UAS-GCaMP6s*; and *247-*
767 *LexA/LexAop-R-GECO* were imaged with an additional excitation laser at 568 nm. Other flies
768 included *UAS-syt-R-GECO/+; APL-Gal4/+*.
769
770 *Imaging data analysis*
771 We separately aligned the imaging data channels using scripts or TurboReg in FIJI. We then
772 drew continuous and even 2-μm ROIs along the neurite. Calcium changes in the ROI were calcu-
773 lated according to the odor delivered. We performed multilayer neurite reconstruction using
774 TrackEM2 in FIJI. The analysis described below was performed in MATLAB. We identified the
775 average calcium signal at 9 s before the odor or electrical stimulus was applied as F_0 and the cal-
776 cium change as $(F- F_0)/F_0$. The peak response 3 times larger than the standard deviation before
777 odor delivery was selected as the responsive ROI, and other points were set to zero. Line traces
778 of APL neurons to different odors represent the mean calicum response plus s.e.m., and statisti-
779 cal analyses were conducted with the Wilcoxon rank-sum test.
780 The angular distance separation between mushroom bodies and APL neurons for eight differ-
781 ent odors was calculated as follows: the peak response of all ROIs (KCs or APL neurons) to one
782 odor represents a vector, and the difference between two vectors was measured by the angle θ
783 between two response vectors (Lei et al., 2013). Thus, the angular distance separation of two
784 odor representations was calculated by 1-cosθ, which ranges from 0 to 1. The average of 28 pairs
785 of odor separation between 8 odors was calculated to measure the separation abilities of KCs and

786 APL neurons. The angular distance separation of different regions of APL neurites was used as
787 the peak response to 8 odors as a vector.
788
789 ***Electrophysiology***
790 Flies were prepared as previously mentioned, with the brain exposed to the air, stably fixed in
791 the chamber, and immersed in ESC. Whole-cell recordings were performed under visual control
792 using an Olympus BX61WI microscope with a 40× water immersion objective. The recordings
793 were performed at 20–25°C with a MultiClamp 700B amplifier (Molecular Devices). The data
794 were low-pass filtered at 10 kHz and acquired at 20 kHz with a Digidata 1440A digitizer (Mo-
795 lecular Devices).
796 Fly brains were dissected and immersed in an extracellular saline solution in a small dish. The
797 saline composition was as follows: 103 mM NaCl, 3 mM KCl, 5 mM N-Tris (hydroxymethyl)
798 methyl-2-aminoethane-sulfonic acid, 10 mM trehalose, 8 mM glucose, 26 mM $NaHCO_3$, 1 mM
799 NaH_2PO_4, 1.5 mM $CaCl_2$, and 4 mM $MgCl_2$ (adjusted to 275 mOsm). The saline was gassed with
800 95% O_2/5% CO_2 to a final pH of 7.3. The sheath covering the target neuron was removed with
801 fine forceps. *GH146-GAL4* was used to label APL neurons. Patch-clamp electrodes (10–20 MΩ)
802 were filled with the following solution: 140 mM potassium aspartate, 10 mM HEPES, 1 mM
803 KCl, 4 mM MgATP, 0.5 mM Na_3GTP, 1 mM EGTA and 1% biocytin hydrazide (pH 7.3, adjust-
804 ed to 265 mOsm). In most of the recorded neurons, a small constant hyperpolarizing current (-
805 50–0 pA) was injected to maintain the membrane potential between −60 and −50 mV. All rea-
806 gents were purchased from Sigma-Aldrich unless stated otherwise. The fly genotype used in this
807 experiment was *GH146Gal4/UAS-tdtomato; 247-LexA/LexAop-NpHr*, n=5.
808

809 ***Immunostaining***

810 Immunostaining was performed as previously reported (Wu & Luo, 2006) with the following
811 modifications: 4-day-old female adult brains were dissected in PBS and then fixed in 4% (wt/vol)
812 paraformaldehyde (Sigma-Aldrich) in PBS on ice for 20 min. After three washes (20 min each)
813 in 0.3% (vol/vol) Triton X-100 (Sigma-Aldrich)/PBS, the samples were blocked with 5%
814 (vol/vol) normal goat serum (NGS, Vector Laboratories) in 0.3% (vol/vol) Triton X-100/PBS for
815 1 h. The samples were then incubated with a primary antibody diluted in 5% NGS in 0.3%
816 (vol/vol) Triton X-100/PBS at 4°C overnight. After three washes (20 min each) in 0.3% (vol/vol)
817 Triton X-100/PBS, the samples were incubated with a secondary antibody diluted in 5% NGS in
818 0.3% Triton X-100 at 4°C overnight. After three washes (20 min each) in 0.3% (vol/vol) Triton
819 X-100/PBS, the samples were mounted with SlowFade Gold antifade reagent (Invitrogen Molec-
820 ular Probes). The primary antibodies included mouse monoclonal nc82 [1:100; Developmental
821 Studies Hybridoma Bank (DSHB)] and rabbit serum anti-GFP (1:500, Invitrogen Molecular
822 Probes). The secondary antibodies included Alexa Fluor 568 goat anti-mouse IgG (1:200, Life
823 Technologies) and Alexa Fluor 488 goat anti-rabbit IgG (1:200, Life Technologies).

824 For imaging, Z-stacks of the brains were acquired on an Olympus FV1000 system with a 60x
825 oil immersion objective at 4× magnification. The volume resolution (xyz) of the mushroom body
826 vertical lobe was 0.077×0.077×0.250 μm^3.

827

828 **Acknowledgements**

829 We thank Ann-Shyn Chiang for kindly offering *APL-GAL4* to us, thank Jean-Paul Vincent for
830 offering *UAS-HRP-mCD8-GFP* lines. We thank Aike Guo (Laboratory of Learning and memory,
831 Institute of Neuroscience, CAS) for his great mentor work, kindly and generously financial sup-

port of this work, and Ke Zhang for his assistance and support. Thank Ji Gang, JianGuo Zhang for EM support (Laboratory of EM, Institute of Biophysics, CAS), Qian Hu for Confocal light microscopy support (Laboratory of Optical Imaging, Institute of Neuroscience, CAS), Hua Han and LiJun Shen for FIJI modification (Laboratory of Microreconstruction, Institute of Automation, CAS). Li Hui for trial of artificial recognition and automatic recognition of neurons (Fudan University). Li Qiang for computing trials for automatic recognition and tracking (Fudan University). Thank ZhengChang Lei for the productive discussion. This work was supported by 973 Program Grant 2011CBA00400 (to A.G.); Natural Science Foundation of China Grants 30921064, 90820008, and 31130027 (to A.G.); and Strategic Priority Research Program of the Chinese Academy of Sciences Grant XDB02040100 (to A.G.).

Competing interest: The authors have no conflicts of interest to declare.

Author contributions

Guangxia Wang designed and performed the calcium imaging experiments, wrote the MATLAB code, analyzed and displayed the calcium imaging and electrophysiological data, and wrote the manuscript. BangYu Zhou and GuangXia Wang designed the EM experiments and synapse-counting experiments and performed the EM experiments. BangYu Zhou and GuangXia Wang worked with ShengXiong Wang, KaiYang, and JianJian Zhao on the reconstructed 3D APL EM connectome data as a team. BangYu Zhou extracted and displayed EM data information. Xing Yang performed the electrophysiology experiment. YiMing Li performed the calcium experiment on the APL output signal in the calyx. LiJun Shen modified the FIJI software. Kai Yang and ShengXiong Wang performed the light microscopy synapse-counting experiment. There is

855 no conflict of interest in this project.

856

857 **References**

858 Aso, Y., Hattori, D., Yu, Y., Johnston, R. M., Iyer, N. A., Ngo, T. T., . . . Rubin, G. M. (2014a).
859 The neuronal architecture of the mushroom body provides a logic for associative learning.
860 *eLife, 3*, e04577. doi:10.7554/eLife.04577

861 Aso, Y., Sitaraman, D., Ichinose, T., Kaun, K. R., Vogt, K., Belliart-Guerin, G., . . . Rubin, G. M.
862 (2014b). Mushroom body output neurons encode valence and guide memory-based action
863 selection in *Drosophila*. *eLife, 3*, e04580. doi:10.7554/eLife.04580

864 Bhattacharya, S., Stewart, B. A., Niemeyer, B. A., Burgess, R. W., McCabe, B. D., Lin, P., . . .
865 Schwarz, T. L. (2002). Members of the synaptobrevin/vesicle-associated membrane
866 protein (VAMP) family in *Drosophila* are functionally interchangeable *in vivo* for
867 neurotransmitter release and cell viability. *Proceedings of the National Academy of*
868 *Sciences of the United States of America, 99*(21), 13867-13872.
869 doi:10.1073/pnas.202335999

870 Briggman, K. L., & Bock, D. D. (2012). Volume electron microscopy for neuronal circuit
871 reconstruction. *Current Opinion in Neurobiology, 22*(1), 154-161.
872 doi:10.1016/j.conb.2011.10.022

873 Chen, T.-W., Wardill, T. J., Yi, S., Pulver, S. R., Renninger, S. L., Amy, B., . . . Vivek, J. (2013).
874 Ultrasensitive fluorescent proteins for imaging neuronal activity. *Nature, 499*(7458), 295-
875 300. doi:10.1038/nature12354

876 Claridge-Chang, A., Roorda, R. D., Vrontou, E., Sjulson, L., Li, H., Hirsh, J., & Miesenbock, G.
877 (2009). Writing memories with light-addressable reinforcement circuitry. *Cell, 139*(2),
878 405-415. doi:10.1016/j.cell.2009.08.034

Cohn, R., Morantte, I., & Ruta, V. (2015). Coordinated and compartmentalized neuromodulation shapes sensory processing in *Drosophila*. *Cell, 163*(7), 1742-1755. doi:10.1016/j.cell.2015.11.019

Cook, S. J., Jarrell, T. A., Brittin, C. A., Wang, Y., Bloniarz, A. E., Yakovlev, M. A., . . . Emmons, S. W. (2019). Whole-animal connectomes of both *Caenorhabditis elegans* sexes. *Nature, 571*(7763), 63-71. doi:10.1038/s41586-019-1352-7

Denk, W., & Horstmann, H. (2004). Serial block-face scanning electron microscopy to reconstruct three-dimensional tissue nanostructure. *PLoS Biology, 2*(11), e329. doi:10.1371/journal.pbio.0020329

Eichler, K., Li, F., Litwin-Kumar, A., Park, Y., Andrade, I., Schneider-Mizell, C. M., . . . Gerber, B. (2017). The complete connectome of a learning and memory centre in an insect brain. *Nature, 548*(7666), 175-182. doi:10.1038/nature23455

Frank, D. D., Jouandet, G. C., Kearney, P. J., Macpherson, L. J., & Gallio, M. (2015). Temperature representation in the *Drosophila* brain. *Nature, 519*(7543), 358-361. doi:10.1038/nature14284

Gianluigi, M., Amit, D. J., & Nicolas, B. (2003). Retrospective and prospective persistent activity induced by Hebbian learning in a recurrent cortical network. *European Journal of Neuroscience, 18*(7), 2011-2024. doi:10.1046/j.1460-9568.2003.02908.x

Goldberg, J. H., Gabor, T., Dmitriy, A., & Rafael, Y. (2003). Calcium microdomains in aspiny dendrites. *Neuron, 40*(4), 807-821. doi:10.1016/S0896-6273(03)00714-1

Grimes, W. N., Zhang, J., Graydon, C. W., Kachar, B., & Diamond, J. S. (2010). Retinal parallel processors: More than 100 independent microcircuits operate within a single interneuron. *Neuron, 65*(6), 873-885. doi:10.1016/j.neuron.2010.02.028

Guo, A., Zhang, K., Ren, Q. Z., Su, H. F., & Chen, N. N. (2016). Functional connectivity mapping of decision-making in *Drosophila melanogaster*. In R. Wang & X. Pan (Eds.), *Advances in Cognitive Neurodynamics (V)* (pp. 35-40). Singapore: Springer Singapore.

Haga, T., & Fukai, T. (2018). Recurrent network model for learning goal-directed sequences through reverse replay. *eLife, 7*, e34171. doi:10.7554/eLife.34171

Hayworth, K. J., Kasthuri, N., Schalek, R., & Lichtman, J. W. (2006). Automating the collection of ultrathin serial sections for large volume TEM reconstructions. *Microscopy & Microanalysis, 12*(S02), 86-87. doi:10.1017/S1431927606066268

Heymann, J. A. W., Hayles, M., Gestmann, I., Giannuzzi, L. A., Lich, B., & Subramaniam, S. (2006). Site-specific 3D imaging of cells and tissues with a dual beam microscope. *Journal of Structural Biology, 155*(1), 63-73. doi:10.1016/j.jsb.2006.03.006

Inada, K., Tsuchimoto, Y., & Kazama, H. (2017). Origins of cell-type-specific olfactory processing in the *Drosophila* mushroom body circuit. *Neuron, 95*(2), 357-367.e354. doi:10.1016/j.neuron.2017.06.039

Joesch, M., Mankus, D., Yamagata, M., Shahbazi, A., Schalek, R., Suissa-Peleg, A., . . . Sanes, J. R. (2016). Reconstruction of genetically identified neurons imaged by serial-section electron microscopy. *eLife, 5*, e15015. doi:10.7554/eLife.15015

Kageyama, G. H., & Meyer, R. L. (1987). Dense HRP filling in pre-fixed brain tissue for light and electron microscopy. *Journal of Histochemistry and Cytochemistry, 35*(10), 1127-1136. doi:10.1177/35.10.3624853

Kasthuri, N., Hayworth, K. J., Berger, D. R., Schalek, R. L., Conchello, J. A., Knowles-Barley, S., . . . Lichtman, J. W. (2015). Saturated reconstruction of a volume of neocortex. *Cell, 162*(3), 648-661. doi:10.1016/j.cell.2015.06.054

Ke, Z., Guo, J. Z., Peng, Y., Wang, X., & Aike, G. (2007). Dopamine-mushroom body circuit regulates saliency-based decision-making in *Drosophila*. *Science, 316*(5833), 1901-1904. doi:10.1126/science.1137357

Kirkhart, C., & Scott, K. (2015). Gustatory learning and processing in the *Drosophila* mushroom bodies. *The Journal of Neuroscience, 35*(15), 5950-5958. doi:10.1523/JNEUROSCI.3930-14.2015

Knott, G., Marchman, H., Wall, D., & Lich, B. (2008). Serial section scanning electron microscopy of adult brain tissue using focused ion beam milling. *Journal of Neuroscience, 28*(12), 2959-2964. doi:10.1523/JNEUROSCI.3189-07.2008

Kohonen, T., & Oja, E. (1976). Fast adaptive formation of orthogonalizing filters and associative memory in recurrent networks of neuron-like elements. *Biological Cybernetics, 21*(2), 85-95. doi:10.1007/BF01259390

Larsen, C. W. (2003). Segment boundary formation in *Drosophila* embryos. *Development, 130*(23), 5625-5635. doi:10.1242/dev.00867

le Magueresse, C., Alfonso, J., Khodosevich, K., Martin, A. A., Bark, C., & Monyer, H. (2011). "Small axonless neurons": Postnatally generated neocortical interneurons with delayed functional maturation. *The Journal of Neuroscience, 31*(46), 16731-16747. doi:10.1523/JNEUROSCI.4273-11.2011

Lee, T., Lee, A., & Luo, L. (1999). Development of the *Drosophila* mushroom bodies: Sequential generation of three distinct types of neurons from a neuroblast. *Development, 126*(18), 4065-4076.

Lei, Z., Chen, K., Li, H., Liu, H., & Guo, A. (2013). The GABA system regulates the sparse coding of odors in the mushroom bodies of *Drosophila*. *Biochemical and Biophysical Research Communications, 436*(1), 35-40. doi:10.1016/j.bbrc.2013.05.036

Li, H., Li, Y., Lei, Z., Wang, K., & Guo, A. (2013). Transformation of odor selectivity from projection neurons to single mushroom body neurons mapped with dual-color calcium imaging. *Proceedings of the National Academy of Sciences of the United States of America, 110*(29), 12084-12089. doi:10.1073/pnas.1305857110

Lin, A. C., Bygrave, A. M., de Calignon, A., Lee, T., & Miesenbock, G. (2014). Sparse, decorrelated odor coding in the mushroom body enhances learned odor discrimination. *Nature Neuroscience, 17*(4), 559-568. doi:10.1038/nn.3660

Liu, Q., Dang, C., & Cao, J. (2010). A novel recurrent neural network with one neuron and finite-time convergence for k-winners-take-all operation. *IEEE Transactions on Neural Networks, 21*(7), 1140-1148. doi:10.1109/TNN.2010.2050781

Liu, X., & Davis, R. L. (2009). The GABAergic anterior paired lateral neuron suppresses and is suppressed by olfactory learning. *Nature Neuroscience, 12*(1), 53-59. doi:10.1038/nn.2235

Macpherson, L. J., Zaharieva, E. E., Kearney, P. J., Alpert, M. H., Lin, T. Y., Turan, Z., . . . Gallio, M. (2015). Dynamic labelling of neural connections in multiple colours by trans-synaptic fluorescence complementation. *Nature Communications, 6*, 10024. doi:10.1038/ncomms10024

Mao, Z., & Davis, R. L. (2009). Eight different types of dopaminergic neurons innervate the *Drosophila* mushroom body neuropil: Anatomical and physiological heterogeneity. *Frontiers in Neural Circuits, 3*, 5. doi:10.3389/neuro.04.005.2009

Marta, R. A., Vitaladevuni, S. N., Yuriy, M., Yuriy, M., Zhiyuan, L., Shin-Ya, T., . . . de Polavieja, G. G. (2011). Wiring economy and volume exclusion determine neuronal placement in the *Drosophila* brain. *Current Biology, 21*(23), 2000-2005. doi:10.1016/j.cub.2011.10.022

Olsen, S. R., & Wilson, R. I. (2008). Lateral presynaptic inhibition mediates gain control in an olfactory circuit. *Nature, 452*(7190), 956-960. doi:10.1038/nature06864

Osinski, B. L., & Kay, L. M. (2016). Granule cell excitability regulates gamma and beta oscillations in a model of the olfactory bulb dendrodendritic microcircuit. *Journal of Neurophysiology, 116*(2), 522-539. doi:10.1152/jn.00988.2015

Papadopoulou, M., Cassenaer, S., Nowotny, T., & Laurent, G. (2011). Normalization for sparse encoding of odors by a wide-field interneuron. *Science, 332*(6030), 721-725. doi:10.1126/science.1201835

Pitman, J. L., Huetteroth, W., Burke, C. J., Krashes, M. J., Lai, S. L., Lee, T., & Waddell, S. (2011). A pair of inhibitory neurons are required to sustain labile memory in the *Drosophila* mushroom body. *Current Biology, 21*(10), 855-861. doi:10.1016/j.cub.2011.03.069

Rall, W. (1969). Time constants and electrotonic length of membrane cylinders and neurons. *Biophysical Journal, 9*(12), 1483-1508. doi:10.1016/S0006-3495(69)86467-2

Ren, Q., Li, H., Wu, Y., Ren, J., & Guo, A. (2012). A GABAergic inhibitory neural circuit regulates visual reversal learning in *Drosophila*. *The Journal of Neuroscience, 32*(34), 11524-11538. doi:10.1523/JNEUROSCI.0827-12.2012

Scholz-Kornehl, S., & Schwarzel, M. (2016). Circuit analysis of a *Drosophila* dopamine type 2 receptor that supports anesthesia-resistant memory. *The Journal of Neuroscience, 36*(30), 7936-7945. doi:10.1523/JNEUROSCI.4475-15.2016

Shu, X., Lev-Ram, V., Deerinck, T. J., Qi, Y., Ramko, E. B., Davidson, M. W., . . . Mcintosh, J. R. (2011). A genetically encoded tag for correlated light and electron microscopy of intact cells, tissues, and organisms. *PLoS Biology, 9*(4), e1001041. doi:10.1371/journal.pbio.1001041

Tanaka, N. K., Tanimoto, H., & Ito, K. (2008). Neuronal assemblies of the *Drosophila* mushroom body. *The Journal of Comparative Neurology, 508*(5), 711-755. doi:10.1002/cne.21692

Tomer, R., Denes, A. S., Tessmar-Raible, K., & Arendt, D. (2010). Profiling by image registration reveals common origin of annelid mushroom bodies and vertebrate pallium. *Cell, 142*(5), 800-809. doi:10.1016/j.cell.2010.07.043

Wang, X. J. (2008). Decision making in recurrent neuronal circuits. *Neuron, 60*(2), 215-234. doi:10.1016/j.neuron.2008.09.034

Wilson, R. I., Turner, G. C., & Laurent, G. (2004). Transformation of olfactory representations in the *Drosophila* antennal lobe. *Science, 303*(5656), 366-370. doi:10.1126/science.1090782

Wong, K.-F. (2006). A recurrent network mechanism of time integration in perceptual decisions. *Journal of Neuroscience, 26*(4), 1314-1328. doi:10.1523/JNEUROSCI.3733-05.2006

Wu, C. L., Shih, M. F., Lai, J. S., Yang, H. T., Turner, G. C., Chen, L., & Chiang, A. S. (2011). Heterotypic gap junctions between two neurons in the *Drosophila* brain are critical for memory. *Current Biology, 21*(10), 848-854. doi:10.1016/j.cub.2011.02.041

1013 Wu, J. S., & Luo, L. (2006). A protocol for dissecting *Drosophila melanogaster* brains for live
1014 imaging or immunostaining. *Nature Protocols, 1*(4), 2110-2115.
1015 doi:10.1038/nprot.2006.336
1016 Wu, Y., Ren, Q., Li, H., & Guo, A. (2012). The GABAergic anterior paired lateral neurons
1017 facilitate olfactory reversal learning in *Drosophila*. *Learning & Memory, 19*(10), 478-486.
1018 doi:10.1101/lm.025726.112
1019 Yang, C. H., Shih, M. F., Chang, C. C., Chiang, M. H., Shih, H. W., Tsai, Y. L., . . . Wu, C. L.
1020 (2016). Additive expression of consolidated memory through *Drosophila* mushroom
1021 body subsets. *PLoS Genetics, 12*(5), e1006061. doi:10.1371/journal.pgen.1006061
1022 Yasuyama, K., Meinertzhagen, I. A., & Schurmann, F. W. (2002). Synaptic organization of the
1023 mushroom body calyx in *Drosophila melanogaster*. *The Journal of Comparative*
1024 *Neurology, 445*(3), 211-226. doi:10.1002/cne.10155
1025 Zheng, Z., Lauritzen, J. S., Perlman, E., Robinson, C. G., Nichols, M., Milkie, D., . . . Sharifi, N.
1026 (2018). A complete electron microscopy volume of the brain of adult *Drosophila*
1027 *melanogaster*. *Cell, 174*(3), 730-743.e722. doi:10.1016/j.cell.2018.06.019